RSC Advances

ROYAL SOCIETY OF CHEMISTRY

www.rsc.org/advances

Journal Name

ARTICLE

Chitosan Assisted Synthesis of 3D Graphene@Au Nanosheets Composites: Catalytic Reduction of 4–nitrophenol

Zhuo Ma,[c] Yunfeng Qiu,[a,b*] Yanmin Huang,[b] Feng Gao,[b] and PingAn Hu[b*]

We report the eco-friendly chitosan assisted synthesis of 3D graphene@Chitosan@Au nanosheets (3DG@CS@AuNSs) composites without using any toxic reductants or capping agents. 3D graphene network consists of few-layer graphene sheets. One the one hand, the interfacial energy between graphene and Au nanostructures is significantly weakened due to the existence of chitosan polymers, serving as "glue" for anchoring Au nanosheets on the surface of 3D graphene. One the other hand, chitosan containing abundant hydroxyl and amine groups act as reducing and stabilizing agents for the formation and even distribution of Au nanosheets. Mild redox reaction between hydrochloroauric ions and hydroxyl and amine groups occurred under thermal condition due to the matching electrochemical potentials of oxidants and reductants. The as-prepared 3DG@AuNSs exhibited much higher activities than that of 3DG@Au nanoaggregates towards the reduction of 4-nitrophenol, as well as more convenient recyclability than other supported Au NPs in terms of robust free-standing foam structure. Furthermore, High performance liquid chromatography was also applied to monitor the emergence of 4-aminophenol during reaction. Present studies not only build a new route for the design of robust and free-standing foam catalyst based on integration of graphene and Au nanostructures by the assistance of natural polymer, but also shed deep insight to the understanding of the synergistic catalytic activity towards nitrophenols.

Introduction

Development of hierarchically three-dimensional (3D) composites has become one of the most attractive subjects in catalysis because most catalytic reactions are diffusion-controlled in a heterogeneous system.[1-3] Many 3D structures have been developed and successfully applied in catalysis, such as zeolites[4], and meso-porous silica[5], carbon[6], and metal oxides[7], macroporous nickel foam[8], flower-like or urchin-like metal oxides[9, 10], etc. These 3D structure can be used as catalysts directly or serve as catalysts supports due to their high surface area for the enhancement of mass transport, the high loading ability for active components, superior absorption ability towards reactants, and unique synergistic effects with catalytic centers.[1, 11] For example, Au nanoparticles loaded on 3D CeO_2 exhibited enhanced catalytic performance towards the oxidation of CO at room temperature.[12] Experimental results have confirmed that localized electrons on the occupied 4f-orbital of Ce^{3+} ions contribute to the electronic interaction between reduced CeO_2 and anchored Au nanoparticles.[13] Taking previous pioneering findings into account, the catalytic properties of Au NPs are dependent on their nanostructures, electronic interaction with supports, and the presence of Au NPs-supports interface.[14] Thus, it is highly appealing to develop promising 3D supports for anchoring hierarchical Au nanostructures to maximize the synergistic effect between them, and render them superior catalytic performance.

Graphene sheets have been widely serving as outstanding supports for anchoring catalysts due to its two-dimensional sheet-like structure, high specific surface area, excellent conductivity, and superior mechanical properties.[15] Reduced graphene oxide (rGO) is regarded as the high throughput and low cost methods to prepare large–scale graphene materials.[16] It has been confirmed that rGO usually suffer from agglomeration and restacking issues because of the Van der Waals interaction, which leads to a great loss of effective surface area, and thus affect the catalytic performance of composites.[17, 18] Furthermore, the residue oxygen groups and defects caused by severe reducing agents always deteriorated the conductivity of graphene, and will eventually affect the electronic interactions with catalytic centers.[19-21] However, graphene prepared by chemical vapor deposition (CVD) method possesses defect free structure, and shows intriguing electronic and catalytic superiorities. Particularly, 3D graphene (3DG) materials have been drawing lots of attention, since they not only maintain the intrinsic properties of 2D graphene sheets, but also provide

a. State Key Laboratory of Urban Water Resource and Environment, Harbin Institute of Technology, Harbin 150090, China. Corresponding author: Fax: +86 451 86403583, E-mail: qiuyf@hit.edu.cn (Y. Qiu).
b. Key Lab of Microsystem and Microstructure, Ministry of Education, Harbin Institute of Technology, No. 2 YiKuang Street, Harbin 150080, PR China. Corresponding author: Fax: +86 451 86403583, E-mail address: hupa@hit.edu.cn (P. Hu).
c. School of Life Science and Technology, Harbin Institute of Technology, 92 West Dazhi Street, Harbin, Heilongjiang, 150001, P.R. China.
† Electronic Supplementary Information (ESI) available: [XPS spectrum of 3DG; SEM images of 3DG@CS@Au synthesized in the presence of 0.05 mg/mL HAuCl₄ and 1 mg/mL HAuCl₄; SEM images of nickel foam@Au; SEM image of 3DG@CS@AuNWs after tenth recycle; Mass spectra of 4-AP; Comparison of the catalytic performances.]. See DOI: 10.1039/x0xx00000x

RSC Advances Accepted Manuscript

superior advantages for the fast transfer of electrolyte ions, and thus might possess great potential to overcome the above–mentioned electron transfer and mass transfer issues.[3, 22, 23] So far, various synthetic strategies for 3DG have been developed including self–assembly, hydrothermal method[24], aerosol[25], template–assisted preparation,[26] and CVD[2]. Among all methods, the preparation of defect-free 3DG by CVD method using nickel foam as template has drawn particular attention. Cheng and coworkers innovatively synthesized 3DG on Ni foam (NF) by CVD, which shows excellent mechanical and electrical properties.[2] The CVD–grown 3DG can provide a highly conductive network due to the highly intrinsic conductivity of defect–free graphene and absence of inter–sheet junction–resistance in seamlessly continuous network. However, the hydrophobic nature of defect-free of 3DG by CVD always causes giant difficulty for the surface modification via non-covalent interactions.[27]

Chitosan (CS) as the second most abundant natural polymer next to cellulose can be prepared from the incomplete deacetylation of chitin[28], showing remarkable properties including good adhesion, high water permeability, superior metal ions coordination ability. CS has been widely used to integrated with Au nanoparticles[29], carbon based materials[30], ionic liquid[31], polyoxometalates[32], etc. to form functional composites by simple preparation methods. In addition, the abundant amino or hydroxyl groups on CS can reduce Au salt precursors under mild conditions due to matching electroactive potentials as confirmed in our previous work.[33] Very recently, wang et. al. demonstrated the surface biomodification of 3DG to prepare enzymatic biosensors by using CS electrodeposition method.[34] Wang's group reported that higher content of Pd(0) and the positive shift of Pd 3d binding energy on TRGO can be realized by the functionalization with CS, leading to the better catalytic performance in DFAFC applications.[35] However, the utilization of CS to anchor Au nanomaterials on CVD-grown 3DG as catalyst for the reduction of 4-NP is seldom investigated.

Herein, we functionalized the large-scale synthesized free-standing 3DG via CVD growth with CS, which serves as ideal 3D support with reducing ability of CS for anchoring Au nanosheets without any other toxic reducing agents under mild conditions. The reduction of nitrophenols, common environmental pollutants due to their toxicity and resistance to microbial degradation, was selected as model reaction to check the catalytic activity of our catalyst. The freestanding, robustness, conductive, and macroporous composites have an enhanced catalytic performance for the reduction of 4-nitrophenol in terms of apparent rate constant and long-term stability as compared to Au aggregates deposited on 3DG directly. High performance liquid chromatography (HPLC) confirmed the generation of 4-aminophenol. Our work not only builds a promising route for anchoring noble metal nanomaterials beyond Au on CVD-growth 3DG with inert surface by introduction of natural polymer, but also shed deep insight to the understanding of the synergistic catalytic activity of nitrophenols.

Experimental section

Materials and methods

Chitosan flakes, from crab shells (Practical grade >85% deacetylated; viscosity < 200 mPa·s) were purchased from Shenyang National Chemical Company. Analytical grade Sodium borohydride ($NaBH_4$), hydrogen tetrachloroaurate hydrate (Hydrochloroauric acid·$3H_2O$), 4–nitrophenol ($C_6H_5NO_3$), $FeCl_3$·$6H_2O$, HCl, Methanol (HPLC grade) and Ethanol (as graphene source) were purchased from Aladdin Industrial Corporation. All compounds were used as received. All solutions were prepared with triply distilled water.

UV–vis spectra were recorded in UV–2550. Scanning electron microscopy (SEM) and energy dispersive X-ray (EDX) spectroscopy measurements were performed on an FEI Quanta 200 scanning electron microscope with 10 kV acceleration voltage. The wavelength and intensity of the laser used for the Raman spectroscopy were 532 nm and 1 mW, respectively (LabRAM XploRA). Agilent Technologies liquid chromatography 1200 series coupled to tandem mass spectrometer Agilent Technologies 6520 series Accurate Mass Quadrupole Time-of-Flight (HPLC-Q-TOF) were used to determine the accurate mass of 4-AP.

Formation of 3DG@Au, nickel foam@Au, and 3DG@CS@AuNSs composites. 3DG is synthesized according to our previous method.[36, 37] 3DG was obtained by etching away nickel foam in 1 M $FeCl_3$ aqueous solution (1 M HCl). 3DG@Au: 3DG foam (1 × 1 cm) was soaked in 2 mL water containing 1 mg/mL $HAuCl_4$·$3H_2O$, and the mixture was incubated for 1h at r.t. 100 μL 0.1 M $NaBH_4$ was injected drop by drop into the above solution to initiate the formation of Au nanostructure. Nickel foam@Au: clean nickel foam (1 × 1 cm) was soaked in 2 mL aqueous solution containing 1 mg/mL $HAuCl_4$·$3H_2O$, and the mixture was incubated at 60 °C for 2 h. 3DG@CS@AuNSs: In a typical procedure, 5 mg chitosan flakes were dissolved in 2 mL 0.2 M acetic acid solution. 3DG foam was soaked in this solution for 1 h, then the pH value of the solution is adjusted to 6.0 ± 0.1 by 1 M HCl and 1 M NaOH aqueous solution. The as-synthesized 3DG@CS was thoroughly washed by distilled water, and was dipped into 2 mL aqueous solution containing 1 mg/mL $HAuCl_4$·$3H_2O$ at 60 °C for 2 h. All final products were thoroughly washed and stored in dark room for future use.

General procedure for the reduction of 4–NP. In a typical reaction, 1 mL of 0.01 mol·L^{-1} 4–NP was added to 2 mL of 0.01 mol·L^{-1} $NaBH_4$ aqueous solution. Subsequently, 10 × 2 mm film was soaked in the solution, and the characteristic absorption peak of 4–nitrophenolate ion at 400 nm gradually decreased. Simultaneously, a new peak at ~295 nm, ascribable to newly generated 4–AP, emerged. The absorption spectra of the solution were recorded in the range of 250–550 nm. The rate constants of the reduction process (k_{app}) were determined using the following equations: $-dC_t/dt = kC_t$ and $\ln(C_t/C_0) = -kt$. The reduction reaction of 4–NP with comparison groups have also been carried out under similar condition.
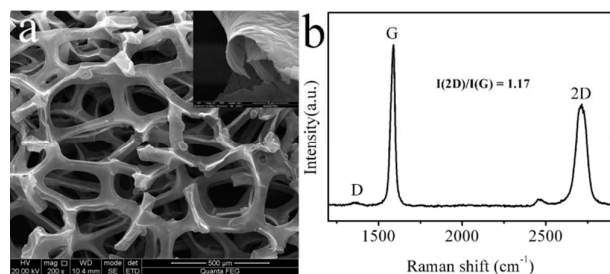
Figure 1. (a) SEM image of 3DG. Inset of (a) is enlarged SEM image of a broken region. (b) Raman spectrum of 3DG foam.

Results and discussion

3DG was synthesized according to previous work via CVD growth using ethanol as carbon source.[2, 36, 37] 3D structure of graphene is clearly shown in **Figure 1a**, which will facilitate the mass transfer during our next heterogeneous catalytic reaction. Enlarged SEM image is shown in the inset of **Figure 1a**, illustrating the thin layer of graphene. In addition, Raman spectroscopy is a powerful characterisation method for graphene, particularly as its profile clearly contains the information of quality and the number of layers. As shown in **Figure 1b**, Raman spectrum shows the characteristic peaks of the G band, D band, and 2D band. Generally, the G band at 1590 cm^{-1} is ascribed to the E_{2g} phonon of C sp2 atoms, while the quite small D band at 1363 cm^{-1} is originating from a breathing mode of a κ-point phonon of A_{1g} symmetry corresponded to local defects and disorder.[38] The small D band intensity displays low defects in as-synthesized graphene, indicative of the high quality. The peak at 2712 cm^{-1} is corresponding to 2D band of graphene. The intensity ratio of G and 2D band is 1.17, implying the 3DG consists of few layer graphene domains. This CVD-growth graphene with less defects endows it high conductivity (0.51 S/cm, measured by four–point probe method) in contrast to the commonly used graphene oxide.[39] In addition, the graphene foam can exist in free-standing structure after etching away the supportive nickel foam due to the excellent mechanical strength of graphene, making it potential to serve as an ideal support for anchoring noble nanostructures. XPS analysis confirmed negligible nickel residues (0.33 wt%) left on the surface after etching process (See **Figure S1** in *SI*).

As is known, the surface of CVD-growth graphene is inert due to hydrophobic chemical nature. Thus, the Au salt precursor (kind of hydrophilic) is difficult to adsorb on its surface, and not mention to form uniform nanostructure for the lack of close interactions. In our preliminary study, 3DG is directly used as support for the deposition of Au nanostructure. As shown in **Figure 2a**, sheet-like Au structures are formed on the surface of graphene framework. The exposed graphene surface clearly shows the incomplete Au film, which are composed of micro-sized Au sheets with curved corners. It is worth noting that the corner is peeled off from the graphene surface spontaneously due to the weak interaction between Au sheets and inert graphene surface. Also, irregular Au nanostructural

surface is formed on the surface of graphene during the reduction of $NaBH_4$. It is assumed that this combined structure might show poor stability during catalytic reactions due to the easy peal-off of Au sheets.

In our previous study[33], we found that CS can enable the successful reduction of $AuCl_4^{-1}$ without any toxic reducing agents under mild conditions. Au nanoparticles are stabilized by CS and show good performance toward the reduction of 4-nitrophenol. Furthermore, it has been proven that CS could be efficiently applied to construct functional composites with reduced graphene oxide and CNT, presenting potential as a good strategy for design of high-performance catalysts.[40, 41] For example, CS modified graphene using a one-step ball milling technique shows enhanced enzyme immobilization capability and electrochemical activity towards the oxidation of glucose.[42]

In our preliminary study, we soaked 3DG into acetic solution with CS concentration of 1 mg/mL. Subsequently, the solution pH value was adjusted to about 7 for thorough precipitation of CS. And the 3DG@CS was thoroughly washed by distilled water. According to our previous preparation protocol, 3DG@CS was incubated in H_4AuCl_4 solution at 50 °C for 2h. As shown in **Figure 2d**, the surface of 3DG is fully covered by Au film, which is composed of porous Au nanostructures. Higher magnification SEM image of Au film displays that porous film consists of interconnected Au sheet. These Au sheets are almost vertically standing on the surface of graphene. The composite film is dissolved into acetic solution for a certain time, and SEM image of centrifuged product is shown in Figure 2f (inset). The thickness of Au film is about 1.5-2 μm. Au mapping of EDS displays the uniform distribution of Au on graphene surface (**Figure 2h**).

It is assumed that CS will stay at the interface between Au film and surface. As shown in **Figure 3a**, the surface of graphene is quite clean, and it becomes rough due to the deposition of a certain amount of CS (**Figure 3b**). The functions of CS during AuNSs synthesis are listed as follows. (1) CS was stuck on graphene surface due to its entangled polymer chains, which serves as binder to anchor $AuCl_4^-$ precursor. (2) The hydroxyl and amine group in CS possess unique reducing ability towards $AuCl_4^-$, which has been confirmed in our previous work. (3)
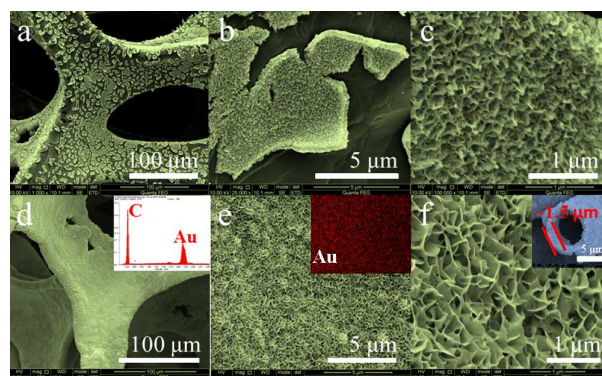

Figure 2. (a, b, and c) SEM images of 3DG@Au from low to high magnification. (d, e, and f) SEM images of 3DG@CS@AuNSs from low to high magnification. Inset of (d) is the EDS. Inset of (e) is the elemental mapping of Au. Inset of (f) is the centrifuged film composed of AuNSs, which is prepared by dissolving foam in acetic acid.
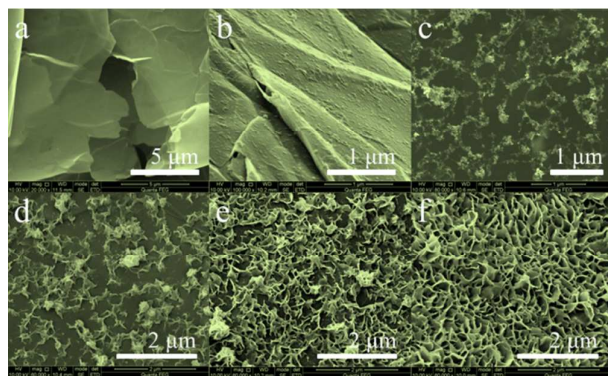
Figure 3. SEM image of (a) pristine graphene sheets of 3DG; (b) CS modified graphene surface of 3DG; 3DG@CS surface with incubation time of (c) 5 min, (d) 20 min, (e) 60 min, and (f) 120 min in the presence of $HAuCl_4$.

The uniform distribution of CS facilitates the homogenous growth of Au nanoparticles (**Figure 3c**), and further catalyse the continuous growth on graphene surface (**Figure 3d** and **3e**). Then Au nanostructure finally turns into interconnected nanosheets due to the confined growing environment of two-dimensional graphene surface and abundant $AuCl_4^-$ precursor in solution (**Figure 3f**). In one word, taking the advantage of CS, AuNSs can be tightly attached to the surface of the 3DG. We also found that the amount of $AuCl_4^-$ precursor played important role in the control of Au morphology. As displayed in **Figure S2a** and **2b**, only irregular Au aggregates are synthesized in the presence of 0.05 mg/mL $HAuCl_4$. In contrast, Au micro-flowers appeared on the surface of AuNSs film when incubated in 1 mg/mL $HAuCl_4$ solution (**Figure S2c** and **2d**).

With the interesting 3DG@CS@AuNSs in hand, we tend to check its performance in the reduction reaction of 4-nitriphenol. As is known, 4-NP can cause inflammation of the eyes, skin, and respiratory tract. Also, it has a delayed interaction with blood to induce methemoglobinemia, potentially causing cyanosis, confusion, and unconsciousness.[43] 4-aminophenol synthesized by the reduction of 4-NP has wide applications as a photographic developer, hair-dying agent, anticorrosion-lubricant, and corrosion inhibitor. Furthermore, 4-AP is an important intermediate for synthesis of various analgesic and antipyretic drugs. Its synthesis can be realized by the reduction of 4-NP by sodium borohydride ($NaBH_4$) with the catalysis of noble metal nanostructures, such as Au nanoparticles, Au nanorods, Au alloys, etc. In particular, Au nanosheets with the least thickness of 15 nm showed high catalytic activity for the reduction of 4-NP to 4-AP.[44] We assume that the combination of 3DG, CS, and AuNSs possess macro- and micro-porous structure, and conductive networks, and tight interface among individual components makes it possible to possess unique catalytic activity towards the reduction of 4-NP.

As shown in **Figure 4a**, a piece of 3DG@CS@AuNSs foam is soaked in 1 mL 4-NP solution with concentration of 0.01 $mol \cdot L^{-1}$, then followed by addition of 2 mL 0.01 $mol \cdot L^{-1}$ $NaBH_4$ aqueous solution. It is clear to see that the colour fades gradually after addition of $NaBH_4$ solution as incubation time increase. This decolouration process can be monitored by

recording the decreasing absorption at 400 nm, which is ascribed to 4–nitrophenolate ion. As seen in **Figure 4b**, the characteristic peak at 400 nm increase significantly with the increasing time, implying the successful reduction of 4-NP. This result confirms that 3DG@CS@AuNSs foam indeed possess catalytic activity for the reduction of 4-NP.

In order to provide deep understanding for the superiority of present catalyst, a comparison study is performed. As shown in **Figure 4c**, C_t/C_0 was plotted versus reaction time, in which C_t is 4-NP concentration at reaction time t, and C_0 is the initial concentration of 4-NP. It is obvious that the reduction of 4-NP doesn't not occur in the absence of catalyst or in the presence of nickel foam. Nickel foam supporting Au is also prepared by in-situ reduction of 0.2 mg/mL $HAuCl_4$ through the redox reaction between nickel and $AuCl_4^-$. In **Figure S3b** and **3c**, Low-magnification and high-magnification SEM images show the nanoflower-like Au aggregates on the surface of nickel foam. In contrast to the profile of C_t/C_0 versus t using 3DG@CS@AuNSs as catalyst, the catalytic activity is obviously lower, confirming the importance of graphene on the enhancement of catalytic performance. The catalytic activity of 3DG@Au (**Figure S4**) is slightly lower than that of 3DG@CS@AuNSs, however it possess poor activity due to the peal-off from the graphene, and also cause recovery issue of catalyst, not mention to the high cost of Au and environmental contamination. We further evaluate the rate constants of the reduction process (k_{app}) according to the above mentioned equation in Experimental section. In our experiment, the concentration of $NaBH_4$ is much higher than that of 4-NP and therefore regarded as unchanged during reaction. Thus, the reduction of 4-NP is hypothesized to be pseudo first-order with respect to the concentration of 4-NP.[45] As plotted in **Figure 4d**, the plots of $ln(C_t/C_0)$ versus reaction time almost display straight line, further implying the
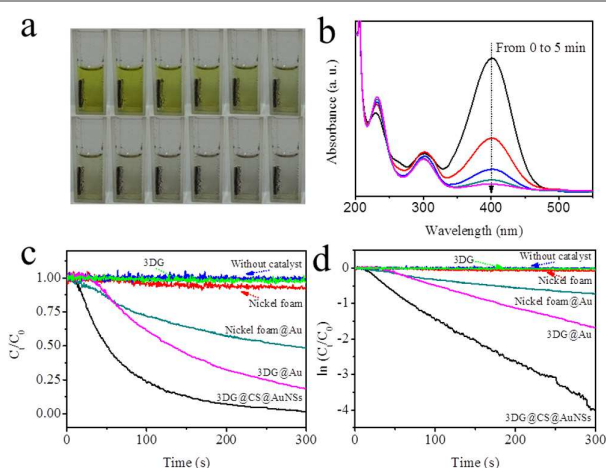

Figure 4. (a) Decolouration process of reaction solution of 4-NP catalyzed by free-standing film of 3DG@CS@AuNSs in the presence of 6.7 mM $NaBH_4$. (b) Successive UV-vis spectra monitoring the reduction of 4-NP (3.3 mM) in the presence of free-standing film of 3DG@CS@AuNSs (10 × 2 mm). (c and d) Plots of C_t/C_0 and $ln(C_t/C_0)$ as a function of time for the reduction of 4-NP (3.3 mM) in the presence of free-standing film of 3DG@CS@AuNSs (size: 10 × 2 mm, black trace), 3DG@Au (size: 10 × 2 mm, pink trace), nickel foam@Au (size: 10 × 2 mm, cyan trace), nickel foam (size: 10 × 2 mm, red trace), 3DG (size: 10 × 2 mm, green trace), and without catalyst (blue trace).
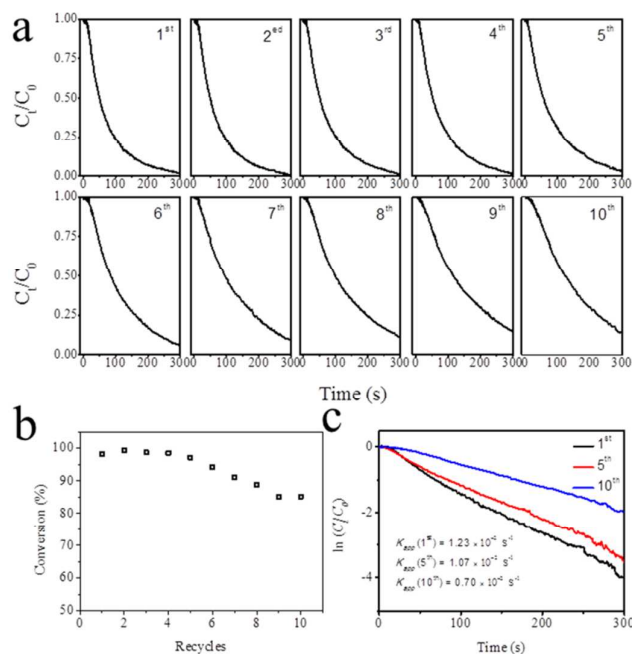
Figure 5. (a) Plots of C_t/C_0 as a function of time for ten recycles at the surface of 3DG@CS@AuNSs. (b) Conversion of 4-NP versus recycle times. (c) and $\ln(C_t/C_0)$ for the reduction of 4-NP (3.3 mM) in the presence of free-standing film of 3DG@CS@AuNSs (size: 10 × 2 mm, black trace).
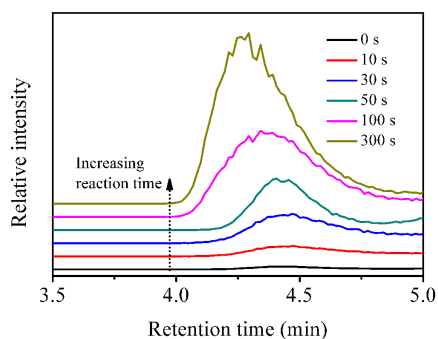

Figure 6. HPLC chromatograms of 4-AP from the reduction of 4-NP for different reaction time monitored at 210 nm ([4-NP] = 3.33 mM, catalyst = 3DG@CS@AuNSs foam (size: 10 × 2 mm)). The slight difference of retention time is caused by manual injection.

hypothesis of the pseudo-first-order equation. k_{app} is thus calculated to be 6.33×10^{-3} S^{-1} for the reaction catalyzed by 3DG@CS@AuNSs. As summarized in **Table S1**, this value is about 1.6 times and 39 times higher than those of 3DG@Au and nickel foam@Au, respectively. k_{app} of 3DG@CS@AuNSs is lower than those of Au NPs/chitosan, Au NPs/chitosan/Fe$_3$O$_4$, Ag/MFC, and POMs@Ag, but our catalyst is a robust free-standing film. This makes it easy to separate from the reaction solution, and can be used in next round by simple washing step using distilled water. In addition, besides the feasibility of recovery, the k_{app} of 3DG@CS@AuNSs is indeed higher than most catalytic systems based on Au, Ag, Pd, Pt, or bimetallic nanoparticles (Table S1 in *SI*). From the above comparison study, the superiority of our catalyst for the reduction of 4-NP is clear to see as we expected based on the
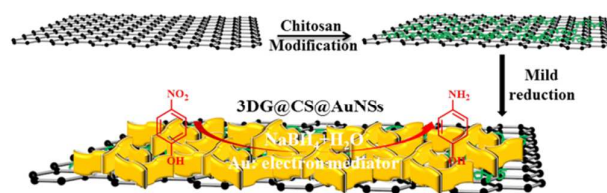
Scheme 1. Schematic illustration of the preparation process of 3DG@CS@AuNSs, and catalytic reduction of 4-NP in the presence of NaBH$_4$.

rationally compositional and structural characteristics. That is to say, as shown in **scheme 1**, the unique interconnected nanostructures of Au nanosheets which provide more available active sites, the improved mass transport by using 3D graphene network as a support. In addition, our catalyst also provide high concentration of 4-NP near catalytic centers, namely Au nanosheets, because of the high absorption ability of graphene towards 4-NP via π–π stacking interactions. Thus, this feature makes the catalyst serving as ideal catalytic environment for the reduction of 4-NP. Furthermore, as shown in SEM images, Au nanosheets were tightly and vertically grown on the surface of 3D graphene by the assistance of chitosan. As is known, the work function of graphene is -4.62 eV, higher than that of Au (-5.1 eV).[46] Therefore, electron transfer from 3D graphene to Au nanosheets will naturally occur due to the matching work functions. This process will concentrate the local electron, rendering the uptake of electrons by adsorbed 4-NP molecules. Briefly, the synergistic effects between Au and graphene, play an important role in the enhancement of catalytic activity.

The reproducible catalytic activity plays a crucial role in practical implementation. In order to evaluate the reusability, ten recycles of the activity were recorded for 3DG@CS@AuNSs in **Figure 5a**. The relative activities versus recycle times are plotted in **Figure 5b**. The 3DG@CS@AuNSs maintains similar catalytic performance without significant loss before seventh recycles (91%) under same reaction conditions, and slightly decreases to 85% at tenth recycle, verifying that the free-standing 3DG@CS@AuNSs foam are stable. In addition, we plot $\ln(C_t/C_0)$ versus reaction time at first, fifth, and tenth recycles in **Figure 5c**, respectively. k_{app} of 3DG@CS@AuNSs decreases from 1.23×10^{-2} S^{-1} at first cycle, to 1.07×10^{-2} S^{-1} at fifth recycle, and then to 0.70×10^{-2} S^{-1} at tenth recycle. As shown in **Figure S5**, AuNSs on grapheme surface maintain intact after tenth recycle, and there are no structural defects found. The loss of catalytic activity might be ascribed to the physical absorption of organic compounds during the course of reaction, and some actively catalytic sites are blocked.

HPLC of the reaction solution further confirms the conversion of 4-NP to 4-AP with respect to reaction time (**Figure 6**). And the high resolution mass spectrum shown in **Figure S6** gives rise to the accurate mass of 4-AP.[47] Taken together, AuNSs on 3DG foam serve as electron mediator between TMB and borohydride ions. Borohydride ions accept an electron donated by Au at the interface of Au and graphene, or on the side surface or edge of AuNSs, turn out to be active surface-hydrogen species. As shown in **Scheme 1**, once the NO$_2$ groups of 4-NP adsorbed on catalyst's surface, reduction is initiated by

these active hydrogen species. However, detailed mechanism for the reduction of 4-NP on the surface of AuNSs needs more in situ spectra technologies. Our preliminary study indeed proves that the combination of 3DG, CS, and AuNSs causes the maximal synergistic effects among all components, which is crucial for the overall enhancement of catalytic reduction activity for 4-NP.

Conclusions

In summary, we demonstrate a facile method for the preparation of 3DG supported AuNSs using CS as binder, as well as stabilization and reduction agent. Due to the tight contact between AuNSs and graphene and unique properties of 3D graphene foam, the as-synthesized free-standing 3DG@CS@AuNSs foam possesses high catalytic activity towards the reduction of 4-NP in the presence of $NaBH_4$. The catalyst shows good stability, facile recovery, and high catalytic performance due to its extraordinary mass transfer pathway, robustness of free-standing structure, maximal synergistic effect among all components. Besides the superior activity towards the reduction of 4–NP, the introduction of biocompatible and biodegradable CS will also endow the catalyst wide applications in bioenzyme mimics or biosensors. Thus, present work builds a useful but simple strategy for the construction of 3D graphene based functional composites.
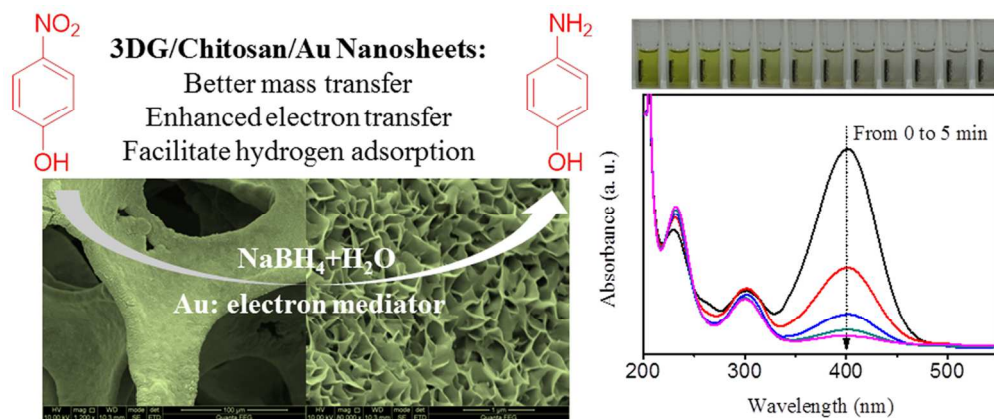
Acknowledgements

Notes and references

1   Z.-S. Wu, S. Yang, Y. Sun, K. Parvez, X. Feng and K. Müllen, *J. Am. Chem. Soc.*, 2012, **134**, 9082-9085.
2   Z. Chen, W. Ren, L. Gao, B. Liu, S. Pei and H.-M. Cheng, *Nat. Mater.*, 2011, **10**, 424-428.
3   W. Chen, S. Li, C. Chen and L. Yan, *Adv. Mater.*, 2011, **23**, 5679-5683.
4   B. Zhao, P. Cheng, X. Chen, C. Cheng, W. Shi, D. Liao, S. Yan and Z. Jiang, *J. Am. Chem. Soc.*, 2004, **126**, 3012-3013.
5   D. Zhao, J. Feng, Q. Huo, N. Melosh, G. H. Fredrickson, B. F. Chmelka and G. D. Stucky, *Science*, 1998, **279**, 548-552.
6   J. Schuster, G. He, B. Mandlmeier, T. Yim, K. T. Lee, T. Bein and L. F. Nazar, *Angew. Chem. Int. Ed.*, 2012, **51**, 3591-3595.
7   Y. Ren, Z. Ma and P. G. Bruce, *Chem. Soc. Rev.*, 2012, **41**, 4909-4927.
8   M. Khairy and S. A. El-Safty, *Chem. Commun.*, 2014, **50**, 1356-1358.
9   M. Ahmad, S. Yingying, A. Nisar, H. Sun, W. Shen, M. Wei and J. Zhu, *J. Mater. Chem.*, 2011, **21**, 7723-7729.
10 B. Wang, H. Wu, L. Yu, R. Xu and T. T. Lim, *Adv. Mater.*, 2012, **24**, 1111-1116.
11 M. J. Allen, V. C. Tung and R. B. Kaner, *Chem. Rev.*, 2009, **110**, 132-145.
12 S. Carrettin, P. Concepción, A. Corma, J. M. López Nieto and V. F. Puntes, *Angew. Chem. Int. Ed.*, 2004, **43**, 2538-2540.
13 H. Y. Kim, H. M. Lee and G. Henkelman, *J. Am. Chem. Soc.*, 2012, **134**, 1560-1570.
14 L. Molina and B. Hammer, *Phys. Rev. Lett.*, 2003, **90**, 206102.
15 A. K. Geim and K. S. Novoselov, *Nat. Mater.*, 2007, **6**, 183-191.
16 O. C. Compton and S. T. Nguyen, *Small*, 2010, **6**, 711-723.
17 Y. Gao, D. Ma, C. Wang, J. Guan and X. Bao, *Chem. Commun.*, 2011, **47**, 2432-2434.
18 D. Zhou and B. H. Han, *Adv. Funct. Mater.*, 2010, **20**, 2717-2722.
19 C. Gómez-Navarro, R. T. Weitz, A. M. Bittner, M. Scolari, A. Mews, M. Burghard and K. Kern, *Nano Lett.*, 2007, **7**, 3499-3503.
20 H. Bai, C. Li and G. Shi, *Adv. Mater.*, 2011, **23**, 1089-1115.
21 J. Shen, Y. Hu, M. Shi, X. Lu, C. Qin, C. Li and M. Ye, *Chem. Mater.*, 2009, **21**, 3514-3520.
22 H. Yin, S. Zhao, J. Wan, H. Tang, L. Chang, L. He, H. Zhao, Y. Gao and Z. Tang, *Adv. Mater.*, 2013, **25**, 6270-6276.
23 L. Jiang and Z. Fan, *Nanoscale*, 2014, **6**, 1922-1945.
24 W. Wei, S. Yang, H. Zhou, I. Lieberwirth, X. Feng and K. Müllen, *Adv. Mater.*, 2013, **25**, 2909-2914.
25 X. Cao, Z. Yin and H. Zhang, *Energy Environ. Sci.*, 2014, **7**, 1850-1865.
26 X. Xie, C. Zhang, M.-B. Wu, Y. Tao, W. Lv and Q.-H. Yang, *Chem. Commun.*, 2013, **49**, 11092-11094.
27 X. Dong, J. Chen, Y. Ma, J. Wang, M. B. Chan-Park, X. Liu, L. Wang, W. Huang and P. Chen, *Chem. Commun.*, 2012, **48**, 10660-10662.
28 F. Shahidi, J. K. V. Arachchi and Y.-J. Jeon, *Trends Food Sci. Technol.*, 1999, **10**, 37-51.
29 C. Sun, R. Qu, H. Chen, C. Ji, C. Wang, Y. Sun and B. Wang, *Carbohydr. Res.*, 2008, **343**, 2595-2599.
30 30.Y. Liu, M. Wang, F. Zhao, Z. Xu and S. Dong, *Biosens. Bioelectron.*, 2005, **21**, 984-988.
31 31.J. Sun, J. Wang, W. Cheng, J. Zhang, X. Li, S. Zhang and Y. She, *Green Chem.*, 2012, **14**, 654-660.
32 D. Fan and J. Hao, *The J. Phys. Chem. B*, 2009, **113**, 7513-7516.
33 Y. Qiu, Z. Ma and P. Hu, *J. Mater. Chem. A*, 2014, **2**, 13471-13478.
34 J. Liu, X. Wang, T. Wang, D. Li, F. Xi, J. Wang and E. Wang, *ACS Appl. Mater. Interfaces*, 2014, **6**, 19997-20002.
35 Y. Wang, H. Liu, L. Wang, H. Wang, X. Du, F. Wang, T. Qi, J.-M. Lee and X. Wang, *J. Mater. Chem. A*, 2013, **1**, 6839-6848.
36 G.-B. Xu, J.-M. Cui, H. Liu, G.-G. Gao, Y.-F. Qiu, S.-M. Zhang and D.-M. Wu, *Electrochim. Acta*, 2015, **168**, 32-40.
37 X. Li, Z. Wang, Y. Qiu, Q. Pan and P. Hu, *J. Alloys Compd.*, 2015, **620**, 31-37.
38 A. Ferrari, J. Meyer, V. Scardaci, C. Casiraghi, M. Lazzeri, F. Mauri, S. Piscanec, D. Jiang, K. Novoselov and S. Roth, *Phys. Rev. Lett.*, 2006, **97**, 187401.
39 X. Cao, Y. Shi, W. Shi, G. Lu, X. Huang, Q. Yan, Q. Zhang and H. Zhang, *Small*, 2011, **7**, 3163-3168.
40 H. Fan, L. Wang, K. Zhao, N. Li, Z. Shi, Z. Ge and Z. Jin, *Biomacromolecules*, 2010, **11**, 2345-2351.
41 C. Shan, H. Yang, D. Han, Q. Zhang, A. Ivaska and L. Niu, *Biosens. Bioelectron.*, 2010, **25**, 1070-1074.
42 W. Zhang, X. Li, R. Zou, H. Wu, H. Shi, S. Yu and Y. Liu, *Scientific reports*, 2015, **5**, DOI: 10.1038/srep11129.
43 O. Isayev, B. Rasulev, L. Gorb and J. Leszczynski, *Mol. Divers.*, 2006, **10**, 233-245.
44 Y. Zhang, Z. Cui, L. Li, L. Guo and S. Yang, *Phys. Chem. Chem. Phys.*, 2015, **17**, 14656-14661.
45 Z. Dong, X. Le, C. Dong, W. Zhang, X. Li and J. Ma, *Appl. Catal. B*, 2015, **162**, 372-380.

46 S. M. Song, J. K. Park, O. J. Sul and B. J. Cho, *Nano Lett.*, 2012, **12**, 3887-3892.
47 N. Daneshvar, M. Behnajady and Y. Z. Asghar, *J. Hazard. Mater.*, 2007, **139**, 275-279.

119x50mm (300 x 300 DPI)